Available online at www.sciencedirect.com
ScienceDirect
Journal of Sound and Vibration 319 (2009) 1067–1082
JOURNAL OF SOUND AND VIBRATION
www.elsevier.com/locate/jsvi

Wall pressure fluctuation spectra due to boundary-layer transition

Sewon Park[a,*], Gerald C. Lauchle[b]

[a]*ITT, Electronic Systems, Naval Command and SONAR Systems, 1810 E-Sara Dr. Chesapeake, VA 23320, USA*
[b]*Retired from Penn State University, Graduate Program in Acoustics, University Park, PA 16802, USA*

Received 17 October 2006; received in revised form 20 May 2008; accepted 20 June 2008
Handling Editor: S. Bolton
Available online 6 August 2008

Abstract

Boundary-layer transition has been expected to be an important contributor to sensor flow-induced self-noise. The pressure fluctuations caused by this spatially bounded, and intermittent, phenomenon encompass a very wide range of wavenumbers and temporal frequencies. Here, we analyze the wavevector–frequency spectrum of the wall pressure fluctuations due to subsonic boundary-layer transition as it occurs on a flat plate under zero-pressure gradient conditions. Based on previous measurements of the statistics of the boundary-layer intermittency, it is found that transition induces higher low-streamwise wavenumber wall pressure levels than does a fully developed turbulent boundary layer that might superficially exist at the same location and at the same Reynolds number. The transition zone spanwise wavenumber pressure components are virtually unchanged from the fully developed turbulent boundary-layer case. The results suggest that transition may be more effective than the fully developed turbulent boundary layer in forcing structural excitation at low Mach numbers, and it may have a more intense radiated noise contribution. This may help explain increases in measured sensor self-noise when the sensors are placed near the transition zone. We believe, based on the presented analytical calculation and numerical simulation, that the rapid growth and subsequent decay of turbulent spots in the intermittent transition zone causes the higher low-(streamwise) wavenumber spectra.

1. Background

Acoustic sensors that are placed flush to the surface of a vehicle are typically used to measure acoustic energy originating from some distant source, such as in sonar applications. If those sensors are placed under the turbulent boundary layer of the vehicle, formed because the vehicle is moving through the medium at some substantial mean speed, U_∞, then the effectiveness of the sensors in capturing the acoustic signals of interest is seriously diminished due to flow-induced sensor self-noise. This self-noise depends strongly on the speed of the vehicle, on whether the turbulent boundary layer is developing in a zero, favorable, or adverse static pressure gradient, and on the proximity of the sensors relative to the beginning and ends of the turbulent boundary layer. If placed near the end of the turbulent boundary layer, the resulting sensor self-noise will have

*Corresponding author. Tel.: +1 757 305 8841.
E-mail address: sewon.park@edocorp.com (S. Park).

0022-460X/$ - see front matter © 2008 Elsevier Ltd. All rights reserved.
doi:10.1016/j.jsv.2008.06.030

significant *additional* contributions due to trailing edge noise mechanisms including possible local flow separation. If the sensors are situated near the beginning of turbulent flow, the laminar-to-turbulent transition zone noise mechanisms contribute. The wall pressure fluctuations generated by turbulent boundary layer, transition zones, separated flows, and edge flows are stochastic fields that have spectral characteristics rich in both frequency and wavenumber content. Wall pressure fluctuations can couple efficiently to the structural modes of the vehicle supporting these flows if the structural modal frequencies and flexural wavenumbers correspond to those of the pressure fluctuations. This adds additional energy to the sensor self-noise spectrum, and also to the radiated noise levels of the vehicle as a whole.

For undersea applications, where the structures are thick and massive, and the mean flow Mach numbers are very low, this coupling occurs predominantly in the so-called *low-wavenumber regime*. At a particular radian frequency, say ω', the majority of the turbulent spectral energy occurs near the convective wavenumber, $k_c \sim \omega'/u_c$, where u_c is the convection speed of turbulent eddies in the boundary layer, typically $\sim 0.7U_\infty$. The acoustic radiation from the turbulence occurs only at sonic and supersonic wavenumbers, $k \leqslant k_o$, where $k_o = \omega'/c_o$ with c_o being the sound speed. Clearly, $k_o/k_c = M_c$, the convective Mach number. In underwater situations, say $U_\infty \sim 15$ m/s, $M_c \sim 10^{-2}$. Two orders of magnitude separate these two important wavenumbers; this range is the low-wavenumber regime. Now if ω' corresponds to a resonant frequency of the vehicle skin, and the wavelength of the corresponding flexural mode is λ_p, then the structural wavenumber at this frequency is $2\pi/\lambda_p$. These wavenumbers invariably reside in the low-wavenumber regime, and it is for this and related reasons, why considerable contemporary research has focused on understanding the low-wavenumber wall pressure fluctuations induced by turbulent boundary layers and related flows. The reader is referred to the books by Howe [1] and Blake [2] for a complete treatment of the issues for zero-pressure gradient turbulent boundary layers, separated, and edge flows. Farabee [3] provides additional comprehensive information on the wall pressure statistics associated with non-equilibrium turbulent boundary layers, while Lauchle [4] reviews the hydroacoustics of boundary-layer transition.

The objective of the work described in this paper is to analyze the wavenumber–frequency characteristics of the wall pressure fluctuations induced by the laminar-to-turbulent transition region on a rigid flat surface under zero-pressure gradient, and very low, subsonic Mach number conditions. We are particularly interested in the low-wavenumber wall pressure components generated by transition, and how they compare to those of the turbulent boundary layer. This analysis provides new information that supports the notion that transition is an important source of both radiated and self-noise for non-rigid vehicles supporting transition in the forward nose region.

2. The transition process

The transition of a laminar boundary layer into a turbulent one is characterized by the breakdown of hairpin vortices into spots of turbulence that are formed randomly in space and time. The spots grow as they convect, and they eventually coalesce to form the turbulent boundary layer. Fig. 1 shows a flow visualization of this process for an axisymmetric body [5].

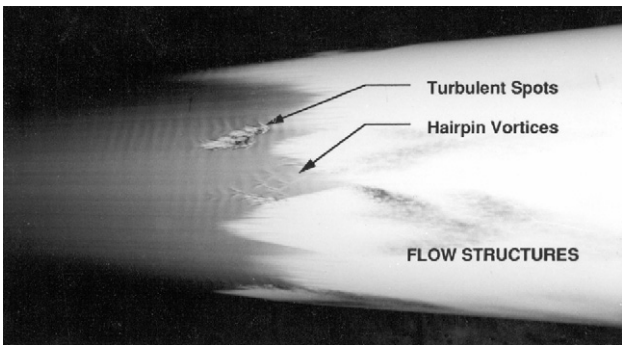

Fig. 1. Visualization of the transition process on an axisymmetric body operating underwater [5].

Following the notations of Dhawan and Narasimha [6] the streamwise distance between the point (at $x_1 = x_o$) in the laminar layer where spots first occur and the beginning of the turbulent boundary layer is called the transition length, Δx. The transition region (or *zone*) is the area covered by turbulent spots, e.g., $L_3\,\Delta x$, where L_3 is the spanwise extent of spot existence. A small pressure transducer located within the transition region generates a signal, $p_{\text{trans}}(x_1, x_3, t)$, that is intermittent—a signal that signifies laminar flow behavior at some instants of time, and turbulent flow behavior at all other instants. The percentage of time that the flow is turbulent at some given in-plane location (x_1, x_3) within the transition region, as determined from a time average of the intermittent signal, is called the intermittency factor, $\gamma(x_1, x_3)$. The intermittent pressure (or velocity or wall shear stress) signal measured in the transition zone can be conditioned electronically [7] to form the intermittency indicator function, $I(x_1, x_3, t)$. The indicator function is a zero–one function; zero when the flow is laminar, and one when the flow is turbulent. Clearly, the time average of $I(x_1, x_3, t)$ is $\gamma(x_1, x_3)$. The burst rate, $N(x_1, x_3)$ is the average number of turbulent spots per unit time that pass the given in-plane location. Fig. 2 schematically illustrates these concepts for a given spanwise position, $x_3 = \text{constant}$.

2.1. Intermittency statistics for boundary-layer transition

Josserand and Lauchle [8] measured the space–time correlation functions of $I(x_1, x_3, t)$ as it occurs naturally in a zero-pressure gradient, flat plate boundary-layer transition zone. They also derived empirical models to describe these correlation functions. If the plate can be considered as infinite in the transverse direction, it is reasonable to let statistical averages of $I(x_1, x_3, t)$ be independent of x_3; however, they are non-homogeneous in the x_1 direction. The definitions of coordinate symbols [8] to be used here are given in Fig. 3.

The time-average value of the intermittency indicator function is the intermittency factor defined as

$$\gamma(x_1) = \lim_{T\to\infty} \frac{1}{T} \int_0^T I(x_1, x_3, t)\,\mathrm{d}t. \tag{1}$$

Josserand and Lauchle [8] investigated the intermittency factor and described the experimental results as

$$\gamma(z_1) = 1 - \mathrm{e}^{(C_3 + C_4 z_1) z_1^2}, \tag{2}$$

where $z_1 = (x_1 - x_o)/\Delta x \equiv \eta_1/\Delta x$, and C_3 and C_4 are, respectively, 1.0 and 3.4.

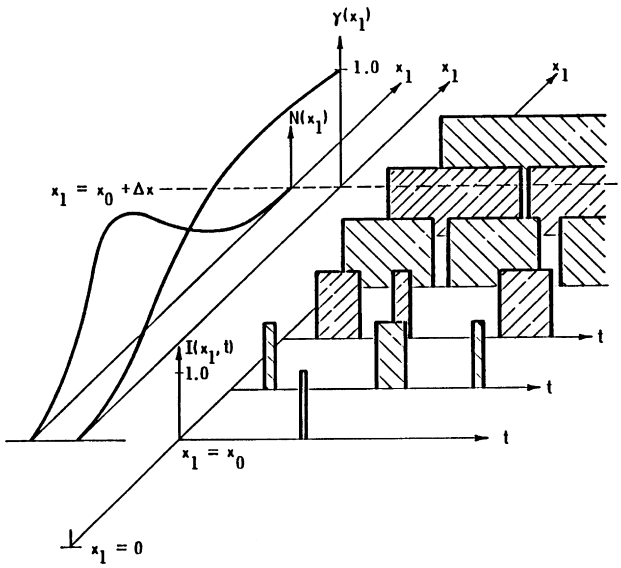

Fig. 2. Intermittency indicator function, $I(x_1,t)$, the burst rate, $N(x_1)$, and the intermittency factor, $\gamma(x_1)$ for some fixed spanwise location in the transition region.

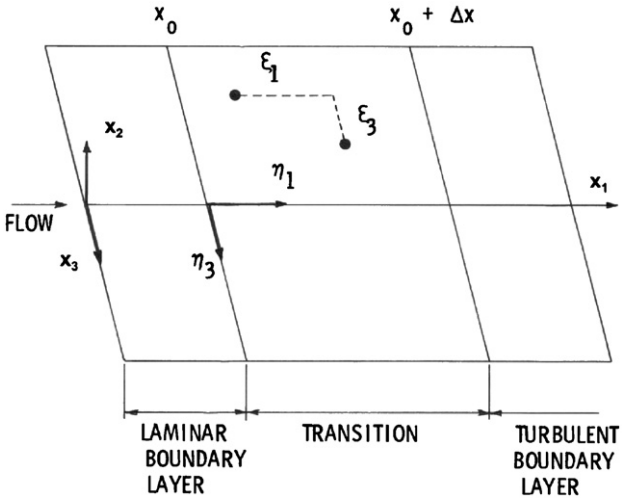

Fig. 3. Definition of coordinates.

Another important statistical property of the intermittency is the spot rate $N(x_1)$. It is described as the mean number of spots that occur at a given streamwise point per unit time. As like the intermittency factor, it is assumed independent of x_3. The non-dimensionalization of the spot rate was first suggested by Farabee et al. [9] and later modified by Gedney and Leehey [10], i.e.,

$$N^*(z_1) = 0.420\left(\frac{\Delta x}{U_\infty}\right)N(z_1). \tag{3}$$

Josserand and Lauchle [8] also found that their experimental data is well described by the Dirac line source hypothesis [10]:

$$N^*(z_1) = C_5\sqrt{(1-\gamma)\ln\left(\frac{1}{1-\gamma}\right)} \tag{4}$$

with $C_5 = 2.38U_\infty/\Delta x$.

The indicator function process is assumed to be independent of that governing the velocity or pressure fluctuations within a single turbulent patch. It is further assumed that the statistics within the patch or spot of turbulence is analogous to that under the fully developed turbulent boundary layer. Therefore, the wall pressure correlation function during transition is modeled as the product of the correlation function of the indicator function, R_I with that of the turbulent boundary layer, R_{Turb}:

$$\langle p_I(\eta_1,\eta_3,t)p_I(\eta_1+\xi_1,\eta_3+\xi_3,t+\tau)\rangle = R_I(\eta_1,\xi_1,\xi_3,\tau)R_{\mathrm{Turb}}(\xi_1,\xi_3,\tau). \tag{5}$$

An empirical model [8] to describe the indicator correlation function is

$$\begin{aligned} R_{rs}(\eta_1,\xi_1,\xi_3,\tau) = {} & \gamma_u\gamma_d + \gamma_u(1-\gamma_d)\exp\left\{-5\left(4+200\left|\tau-\frac{\xi_1}{U_c}\right|\right)\left|\tau-\frac{\xi_1}{U}\right|\right\} \\ & \times\exp\left(20\frac{|\Lambda_1|}{0.014+|\Lambda_1|}\left|\tau-\frac{\xi_1}{U}\right|\right)\exp\left(-\left|15.75\Delta x-\frac{1260|\tau-\xi_1/U|}{1+71|\Lambda_3|}\right|\frac{|\Lambda_3|}{1+14.2|\Lambda_1|}\right) \\ & \times\exp\left(-\frac{A|\Lambda_1|}{0.0014+|\Lambda_1|}\frac{1}{1+1300|\tau-\xi_1/U_c|}\right). \end{aligned} \tag{6}$$

Here, subscript u refers to the upstream sensor location and d to the downstream sensor location. For an upstream reference location, $\gamma_u = \gamma(\eta_1)$ and $\gamma_d = \gamma(\eta_1+\xi_1)$. These are reversed for a reference location that is

downstream of the second sensor. The other symbols in this equation are Λ_1 $(\Lambda_3) = \xi_1$ $(\xi_3)/\Delta x$ and $A = -\ln[1-\exp(-4.27/\Delta x)]$ with Δx in meters.

3. The wavevector–frequency spectrum for boundary-layer transition wall pressure fluctuations

Wavevector spectrum analysis is a very powerful tool to identify the characteristics of the signal for a homogeneous field signal. For the infinitely wide plate, the transition zone statistics can be assumed to be homogeneous in the spanwise direction. But by its very nature, boundary-layer transition has statistics that are inhomogeneous in the streamwise direction. This is because the statistically averaged flow variables change from those of a laminar state to those of a turbulent one. This stochastic process is described formally as one that is *weakly non-homogeneous*. Analogously to time–frequency analysis for a weakly non-stationary temporal process, where waterfall analysis may be utilized, wavevector–frequency spectral analysis (with varying reference position) may be used in the weakly non-homogeneous process. Such analysis can capture the wavenumber and frequency spectral changes throughout the field.

3.1. Implementation

The wall pressure wavevector–frequency spectrum for the transition zone wall pressure fluctuations can be calculated directly from Eq. (5) by Fourier transforming over both space and time. In particular, we find

$$\Phi_{rs}^{\mathrm{Tran}}(\eta, k_1, k_3, \omega) = \Phi_{rs}^{I}(\eta, k_1, k_3, \omega) * \Phi_{rs}^{\mathrm{Turb}}(k_1, k_3, \omega). \tag{7}$$

The asterisk symbol indicates convolution of the transition zone intermittency indicator function spectrum with that of a fully developed turbulent boundary layer. Subscript r refers to the reference sensor and s to the second sensor. Each time–space correlation function and wavenumber–frequency spectrum pair is related as

$$\Phi(\eta, k_1, k_3, \omega) = \frac{1}{(2\pi)^3} \int_{-\infty}^{+\infty} \int_{-\infty}^{+\infty} \int_{-\infty}^{+\infty} R(\eta, \xi_1, \xi_3, \omega) \mathrm{e}^{-\mathrm{i}(k_1\xi_1 + k_3\xi_3 - \omega\tau)} \, \mathrm{d}\xi_1 \, \mathrm{d}\xi_3 \, \mathrm{d}\tau. \tag{8}$$

The turbulent boundary-layer wavevector–frequency spectrum is relatively well known and can be obtained from many different sources in the contemporary literature. We use the Corcos [11] model because of its simplicity and ease of implementation. To calculate the wall pressure wavevector–frequency spectrum in the transition zone from Eq. (7), we need to first substitute Eq. (6) into Eq. (8) and evaluate the transform.

3.2. Indicator function wavevector–frequency spectrum

The dual relationship between the space–time correlation function and the wavevector-frequency spectrum is the three-dimensional Fourier transform given by Eq. (8). In this research, numerical processing is performed spanwise and streamwise, separately. Therefore, only two-dimensional (2-D) Fourier transforms are required (one in space and one in time), which leads to two separate *wavenumber*–frequency spectra. For the streamwise direction, we have

$$\Phi(\eta, k_1, \omega) = \frac{1}{(2\pi)^2} \int_{-\infty}^{+\infty} \int_{-\infty}^{+\infty} R(\eta, \xi_1, 0, \tau) \mathrm{e}^{-\mathrm{i}(k_1\xi_1 - \omega\tau)} \, \mathrm{d}\xi_1 \, \mathrm{d}\tau \tag{9}$$

and for the spanwise direction:

$$\Phi(\eta, k_3, \omega) = \frac{1}{(2\pi)^2} \int_{-\infty}^{+\infty} \int_{-\infty}^{+\infty} R(\eta, 0, \xi_3, \tau) \mathrm{e}^{-\mathrm{i}(k_3\xi_3 - \omega\tau)} \, \mathrm{d}\xi_3 \, \mathrm{d}\tau. \tag{10}$$

Accurate numerical evaluation of these transforms requires that the limits of integration be truncated to finite values, and that the sampling functions are chosen to prevent aliasing in both the frequency and wavenumber domains. Because the space–time correlation functions are developed from experimental data [8] collected in air over a given finite area of a test plate, the spatial limits and increments are chosen to correspond to those of the experimental transducer array. That is, $\Delta\xi_1 = \Delta\xi_3 = 2.54$ cm. These uniform spatial sampling increments result in un-aliased wavenumber spectra [12,13] for $k_1(k_3) = \pi/\Delta\xi_1(\Delta\xi_3)$, i.e.,

$|k_1, k_3| = 123\,\text{rad/m}$. In accordance to the experimental array size, 41 spatial samples are chosen in the stream and spanwise directions. The temporal sampling frequency is set at 250 Hz, which results in un-aliased frequency domain spectra for $f < 125\,\text{Hz}$; the frequency selected in Ref. [8].

The correlation values computed from Eq. (6) must approach zero smoothly as the limits of integration are exceeded. This is accomplished by windowing. In the transformed domains, the selected window function should have low sidelobes in order to minimize sidelobe leakage into the spectral results that can distort the true wavenumber content of the pressure fluctuations. This can be accomplished with many window functions, but at the cost of broadening the mainlobe. This diminishes the spectral resolution. Because this research involves the pressure field of an intermittent turbulent layer, known to contain broadband energy levels, but concentrated in specific regions of the wavenumber–frequency domain, the resolution issue is deemed less important than the sidelobe leakage problem. Therefore, a Taylor weighting function [12,14] was used, for both the spatial and temporal windows. This weighting function is

$$w(p) = \frac{1}{2\pi}\left\{F(0) + 2\sum_{m=1}^{\bar{n}-1} F(m)\cos(mp)\right\}, \quad |p| \leqslant \pi,$$

$$F(m) = \prod_{n=1}^{\bar{n}-1}\left[\frac{1 - m^2/\sigma^2(A^2 + (n-1/2)^2)}{1 - m^2/n^2}\frac{\sin(\pi m)}{\pi m}\right],$$

$$\sigma = \frac{\bar{n}}{\sqrt{A^2 + \left(\bar{n} - \frac{1}{2}\right)^2}}, \quad A = \frac{1}{\pi}\ln\left(R + \sqrt{R^2 - 1}\right), \quad R = 10^{|S|/20}. \tag{11}$$

Taylor weighting is known to make the first few sidelobes near the mainlobe nearly flat [14]. The parameter S controls the sidelobe level in dB, and the parameter n controls the number of the nulls. We choose $S = 60\,\text{dB}$ and $\bar{n} = 2$.

The windowing operation effectively suppresses sidelobe leakage, but it also introduces the unavoidable effect of spectral amplitude reduction. A window calibration factor is thus used to preserve the original power of the signal. This is explained qualitatively as follows. If both the reference and second probe are located under the turbulent boundary layer, then the indicator function is unity and the 2-D Fourier transform of this function would be a product of two unit delta functions. When convolved with the turbulent boundary-layer spectrum, according to Eq. (7), we obtain the desired result: the wavevector–frequency spectrum of the turbulent boundary-layer wall pressure fluctuations. But, if we perform this process with a window, the 2-D Fourier transform of the windowed indicator function mimics a pair of delta functions, but they have magnitudes greater than unity (by about 1.4%). Consequently, the convolution results in a magnitude error for the turbulent boundary-layer spectrum. A narrowband window calibration factor is thus required to compensate for this effect. This factor is calculated in the wavenumber–frequency domain to preserve the overall magnitude of the original signal. First, a 2-D FFT is performed on the Taylor window function, and the power sum of the values in each wavenumber (or frequency) bin is compared with the 2-D FFT for a uniform function of unit amplitude. The ratio of these two computations is then multiplied, bin-by-bin, with the required 2-D FFTs calculated using the window.

3.3. Transition zone wall pressure spectrum

The wavenumber–frequency spectrum of the wall pressure fluctuations under the transition zone is calculated from the convolution described by Eq. (7), using the Taylor windowed spectrum of the indicator function. In the streamwise direction, we have

$$\Phi_{rs}^{\text{Tran}}(\eta, k_1, \omega) = \Phi^{I}(\eta, k_1, \omega) * \Phi^{\text{Turb}}(k_1, \omega) \tag{12}$$

and for the spanwise direction:

$$\Phi_{rs}^{\text{Tran}}(\eta, k_3, \omega) = \Phi^{I}(\eta, k_3, \omega) * \Phi^{\text{Turb}}(k_3, \omega), \tag{13}$$

where the $\Phi_{1,2}$ spectra are computed using the procedures of Section II-B. The Corcos [11] models for the turbulent boundary-layer wall pressure wavenumber–frequency spectra are:

$$\Phi^{\mathrm{Turb}}(k_1,\omega)=\frac{l_1}{\pi}\left(\frac{\sqrt{\Phi(\omega)}}{1+l_1^2(k_1-k_c)^2}\right),\quad \Phi^{\mathrm{Turb}}(k_3,\omega)=\frac{l_3}{\pi}\left(\frac{\sqrt{\Phi(\omega)}}{1+l_3^2k_3^2}\right), \tag{14}$$

where $\Phi(\omega)$ is the point wall pressure spectrum, and the correlation lengths are:

$$l_1=\frac{u_c}{\varepsilon_1\omega},\quad l_3=\frac{u_c}{\omega}. \tag{15}$$

Here, $\varepsilon_1=0.17$ and convective wavenumber $k_c=\omega/u_c=1/l_1\varepsilon_1$.

4. Results

Calculations are performed in MATLAB®, where the 2-D FFT and convolution operations are functions provided in this software package. Fig. 4 shows the streamwise space–time correlation function of the indicator function calculated using Eq. (6) and $\xi_3=0$. These correlations are shown for four (4) reference positions within $0.2\leqslant z_1\leqslant 0.9$. The temporal variable ranges from -1 to 1 s with a time increment of 4 ms, and the spatial variable ranges from 0.508 m upstream to 0.508 m downstream in 2.54 cm increments. This range encompasses the entire transition zone measured by Josserand and Lauchle [8] at a free-stream velocity of 11.77 m/s (in air). The angled highlight in the center of the plots is indicative of the turbulent spots being

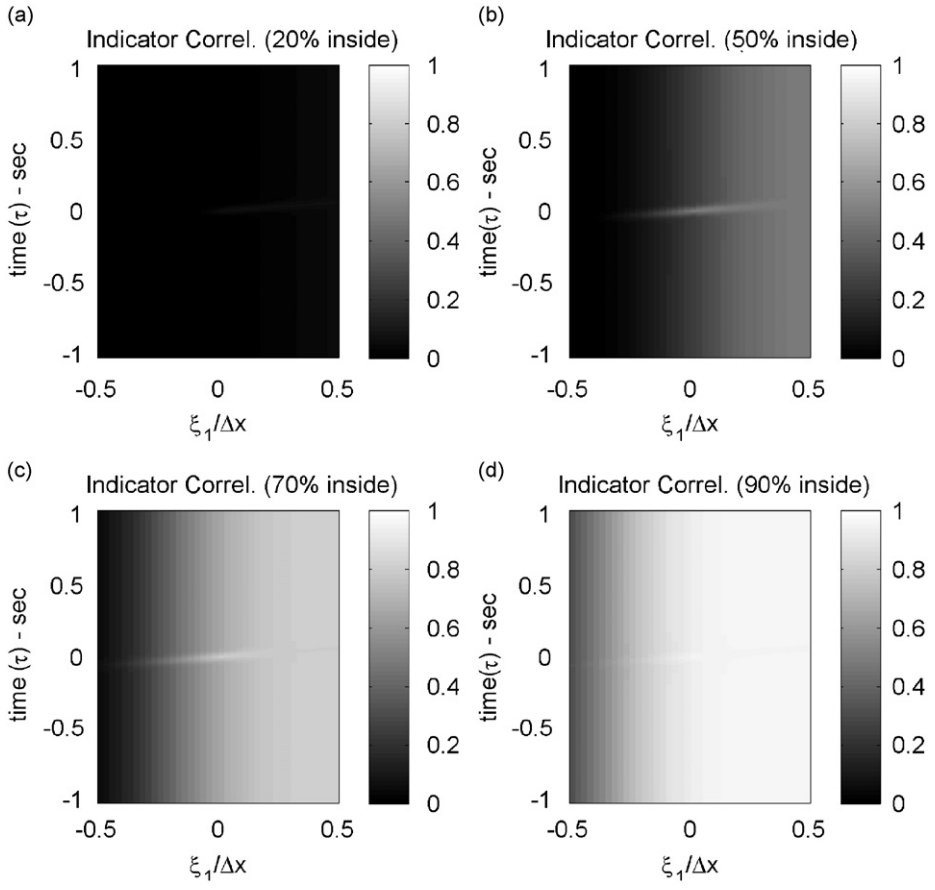

Fig. 4. Calculated streamwise space–time correlation functions for transition zone intermittency function, $R_I(\eta_1,\xi_1,0,\tau)$ with $0.2\leqslant z_1\leqslant 0.9$. ξ_1 is distance from the reference in streamwise direction. Δx is the length of the transition zone.

convected at a speed slightly smaller than the free-stream velocity. This is not a pure line, but is smeared because not all spots travel at the same speed. Furthermore, the respective leading and trailing edges of the spots also travel at different speeds. At large delay times the correlation function approaches $(\gamma_r\gamma_s)^{1/2}$, so the color contrast of the plots at the upper and lower borders follow the same functional behavior as γ_s through the range of ξ_1, weighted by the value of γ_r. This is further indicated by the plots becoming lighter as we progress from $z_1 \sim 0$ to $z_1 \sim 1$.

At each reference position, the wavenumber–frequency spectrum is calculated, Fig. 5. For a reference position that is 30% into the transition zone, Fig. 5(a) shows the correlation function for the indicator function, and Fig. 5(b) shows the streamwise wavenumber–frequency transformation of this function with no windowing operation performed. The space–time characteristics of the Taylor window function, Eq. (11), are shown in Fig. 5(c). Now when this window function is multiplied by the indicator correlation function, a windowed indicator correlation function is created as shown in Fig. 5(d). The streamwise wavenumber–frequency spectrum of this windowed indicator function is shown in Fig. 5(e). The suppression of sidelobe leakage, in *both* frequency and wavenumber, through use of the window function is clearly observed when comparing Fig. 5(b–e).

In Fig. 6 we compare the wavevector–frequency spectra for the fully developed turbulent boundary layer with that of the transition zone at a reference location 30% into the zone. The flow conditions are assumed identical for each of these calculations, the levels are normalized by $\Phi(\omega)$, so the spectrum levels presented here have the units of meters per radian. Eq. (14) is used for Fig. 6(a and c), while Eqs. (12) and (13) are used for

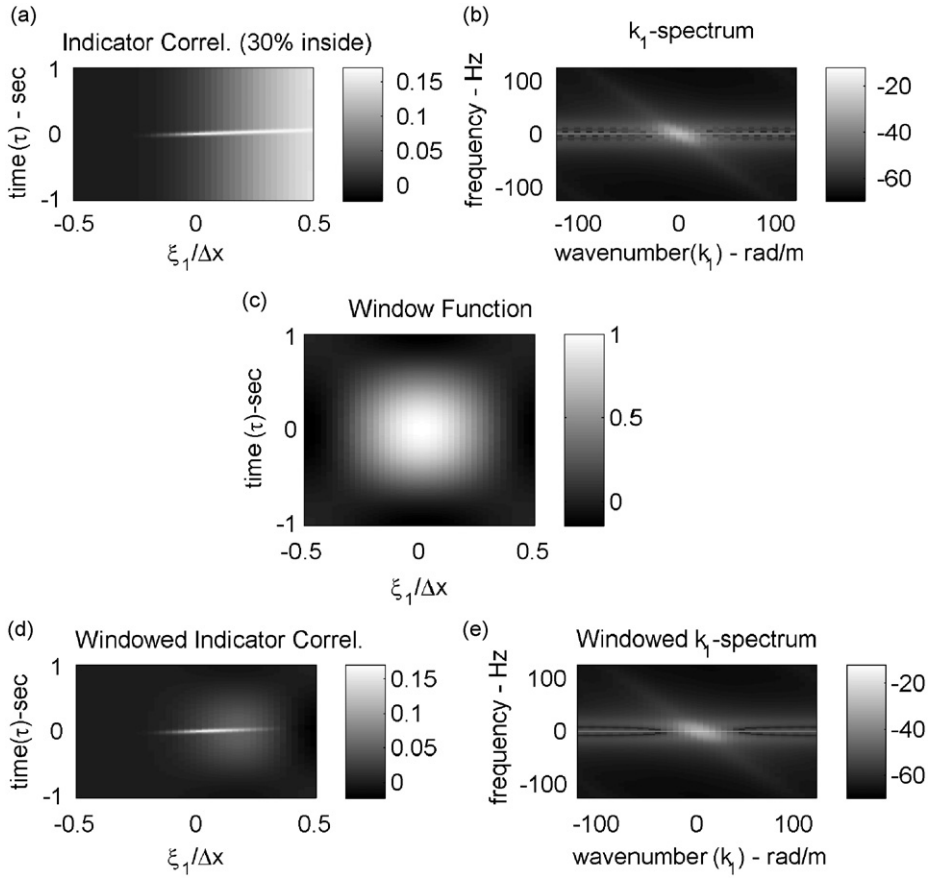

Fig. 5. Processing steps for calculating the streamwise wavenumber–frequency spectrum (for $z_1 = 0.3$); (a) space–time correlation function for the indicator function; (b) 2-D FFT of correlation shown in (a); (c) the Taylor weighting function; (d) correlation function for the indicator function after application of the Taylor window; (e) streamwise wavenumber–frequency spectrum of the indicator function after the necessary windowing operation. ξ_1 is distance from the reference in streamwise direction. Δx is the length of the transition zone.

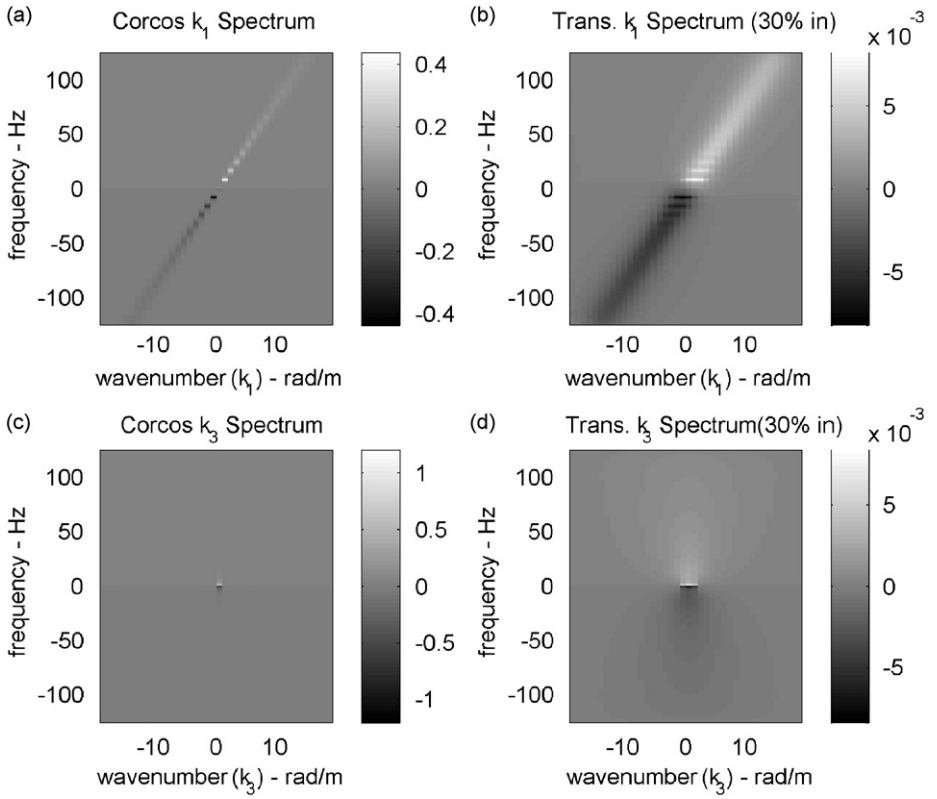

Fig. 6. Turbulent boundary-layer wall pressure wavevector–frequency spectrum [11] compared to that under a transitional boundary layer on a flat plate operating at zero incidence in air at 11.77 m/s: (a) $k_1-\omega$ spectrum of the turbulent boundary layer; (b) $k_1-\omega$ spectrum for transition; (c) $k_3-\omega$ spectrum of the turbulent boundary layer; (d) $k_3-\omega$ spectrum for transition.

Fig. 6(b and d), respectively. The Taylor window is applied throughout. There is apparently higher low-wavenumber energy created in the transition zone than in the turbulent boundary layer as indicated by lighter highlights along the convective ridge in the $\omega-k_1$ plots. This feature can be visualized easier by cross-plotting the spectrum level at constant frequency with wavenumber.

Fig. 7 shows the non-dimensional $k_1-\omega$ spectra for both the turbulent boundary layer and the transition zone at various reference locations, and for four (4) discrete frequencies [the spectrum level is normalized with $\Phi(\omega)/k_c$]. As the reference position moves downstream, the low k_1-wavenumber spectral content increases over that of the turbulent boundary layer. This effect is observed for all of the considered frequencies, but it is especially noticeable at the lower frequencies.

In Fig. 8, we show the spanwise wavenumber spectra at the four (4) constant frequencies in the same format as Fig. 7. Clearly, the transition zone wall pressure $k_3-\omega$ spectrum is virtually identical to that of the fully developed turbulent boundary layer for $z_1 = 0.9$. For smaller values of z_1, the transition zone spectral levels decrease in proportion to the intermittency factor.

5. Discussion

In the context of boundary-layer transition, intermittency means fluctuation between a laminar state and a turbulent one. In a fully developed turbulent boundary layer, high-pressure fluctuations are believed to be caused by the formation and decay of coherent structures. Conceptually, the magnitude of a pressure fluctuation between a laminar state and a turbulent one (as in transition) is expected to be significantly larger than the magnitude of a fluctuation between a coherent burst within a turbulent boundary layer and the surrounding turbulent flow. That is, the growth and decay of coherent structures within a turbulent boundary

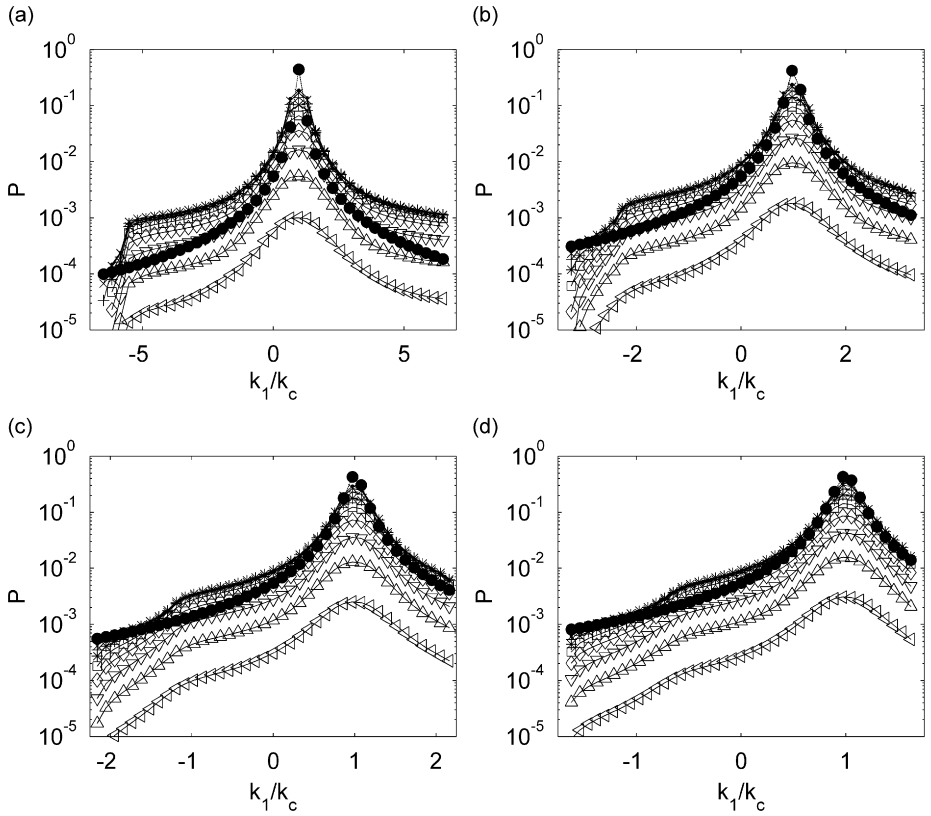

Fig. 7. Non-dimensional k_1-ω spectra at various frequencies, and for $0.1 \leqslant z_1 \leqslant 0.9$; ($\lhd$) $z_1 = 0.1$, ($\triangle$) $z_1 = 0.2$, ($\bigtriangledown$) $z_1 = 0.3$, ($\diamond$) $z_1 = 0.4$, ($\square$) $z_1 = 0.5$, ($*$) $z_1 = 0.6$, ($+$) $z_1 = 0.7$, ($\times$) $z_1 = 0.8$, ($\bullet$) $z_1 = 0.9$, and $\bullet$ indicates the turbulent boundary-layer wavenumber spectrum [11]; P is power spectral density (normalized with point wall pressure spectra), k_1 is streamwise wavenumber and k_c is convective wavenumber; frequencies (a) 25 Hz; (b) 50 Hz; (c) 75 Hz; (d) 100 Hz.

layer will not produce pressure fluctuations of comparable magnitude to those produced by the growth and decay of turbulent spots within a laminar boundary layer. The reason is that the pressure fluctuation in the laminar state is essentially zero, while there is always a residual (greater than zero) pressure fluctuation in a turbulent boundary layer at those locations not occupied by a coherent structure. So, within the transition zone, we might expect higher wall pressure fluctuation levels. The $k_1-\omega$ spectra of the transition zone wall pressure fluctuations presented here indicate that the low-wavenumber components are higher than those of a turbulent boundary layer that might exist superficially at the same location and Reynolds number. The increase occurs when $z_1 = 0.5$ which happens to correspond to the peak in the burst rate distribution [$N(x_1)$, Eq. (4)]. The peak in the burst rate would imply a more energetic state, of higher intermittency, and hence, of higher level low-wavenumber pressure fluctuation. This effect is not only borne out by the calculations presented here, but also by the experimental results of Audet et al. [15] and Dufourcq [16]. They measured the local rms wall pressure fluctuations under a flat plate boundary-layer transition zone, as a function of streamwise position. They found a high-level peak in the pressure fluctuation at approximately 50% into the transition zone ($z_1 = 0.5$).

A new explanation for why boundary-layer transition intermittency and discontinuous turbulence may give rise to low wavenumber energy and sound radiation is given by Sandham et al. [17]. They consider the radiation from exponentially growing and decaying subsonic traveling waves. Although their primary interest is in the radiation from subsonic jets, they mention that their model may also be applicable to boundary-layer transition. We will presently demonstrate their approach using numerical simulations of both the turbulent boundary-layer and transition zone wall pressure fluctuations.

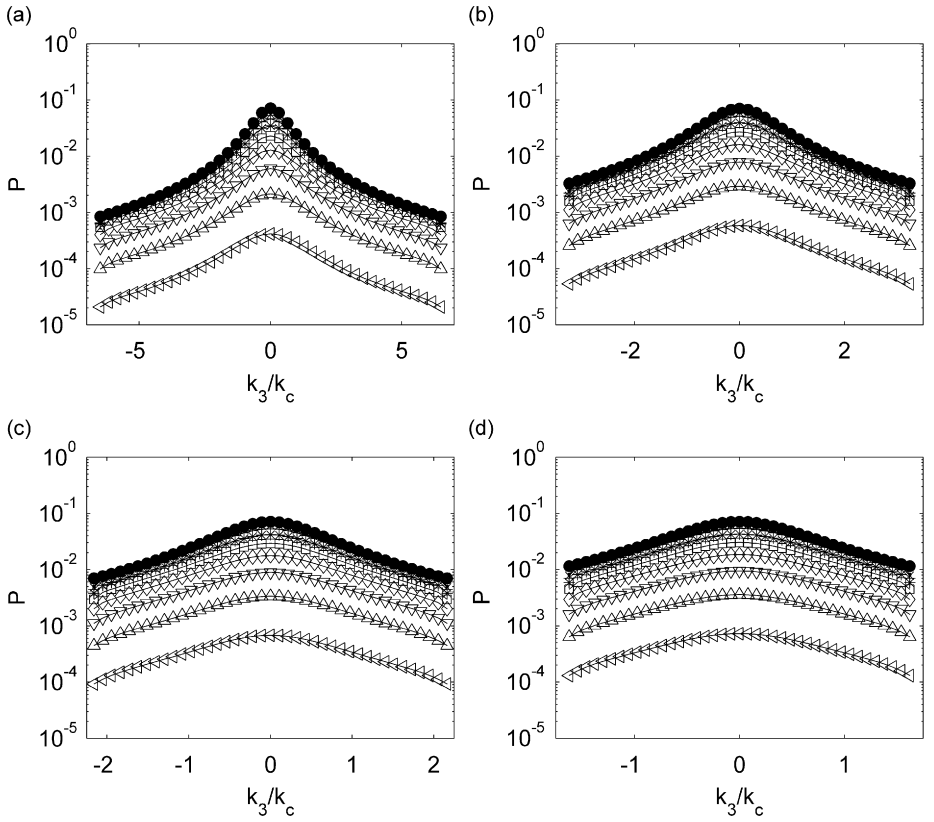

Fig. 8. Spanwise non-dimensional k_3–ω spectra at various frequencies for $0.1 \leqslant z_1 \leqslant 0.9$; ($\triangleleft$) $z_1 = 0.1$, ($\triangle$) $z_1 = 0.2$, ($\triangledown$) $z_1 = 0.3$, ($\diamond$) $z_1 = 0.4$, ($\square$) $z_1 = 0.5$, ($*$) $z_1 = 0.6$, ($+$) $z_1 = 0.7$, ($\times$) $z_1 = 0.8$, ($\bullet$) $z_1 = 0.9$, and $\bullet$ indicates the turbulent boundary-layer wavenumber spectrum [11]; P is power spectral density (normalized with point wall pressure spectra) and k_3 is spanwise wavenumber; (a) 25 Hz; (b) 50 Hz; (c) 75 Hz; (d) 100 Hz.

5.1. Semi-mathematical model of the wall pressure spectrum inside of the transition region

We consider a wavenumber white wall pressure disturbances transported in the x-direction at convection velocity U_c:

$$p(x,t) = \sum_K A(k) e^{ik(x-U_c t)}. \tag{16}$$

The 2-D Fourier transform of Eq. (16) gives

$$p(k,\omega) = \iint \sum_K A(k) e^{ik(x-U_c t)} e^{i\omega t} e^{ikx}\, dt\, dx = A(k)\delta(ku_c - \omega). \tag{17}$$

When the growth (or decay) function, $G(t)$, of Sandham et al. [17] is applied to Eq. (16), we have a simulation of transition, e.g.,

$$p(x,t) = \sum_k A(k) e^{ik(x-U_c t)} G(t). \tag{18}$$

Fourier transform of Eq. (18) results in

$$p(k,\omega) = A(k) \int G(t) e^{i(\omega - kU_c)t}\, dt. \tag{19}$$

The integral is not the same as $\delta(\omega - kU_c)$, because of the function $G(t)$. Consider a Gaussian function for $G(t)$, which is a good representation for a growing and decaying field:

$$G(t) = e^{-at^2}. \tag{20}$$

The Fourier transform can be expressed as

$$p(k,\omega) = A(k)\int e^{-at^2} e^{-i(kU_c-\omega)t}\,dt = A(k)\sqrt{\frac{\pi}{a}} e^{-\pi^2(ku_c-\omega)^2/a}. \tag{21}$$

The above result shows that the wavenumber component at $k = k_c = \omega/U_c$ spreads to the neighbor wavenumber components, as suggested in Fig. 7 for boundary-layer transition.

Eqs. (16)–(21) are now used for the simulation of turbulent flow on the flat plate, and the wavenumber spreading effect in a transition region. We consider the case of multiple disturbances growing and decaying while being transported by the mean flow. Eq. (16) for a turbulent boundary layer is represented by

$$p(x,t) = \sum_k A(k) e^{ik(x-U_c t)+\theta_k}, \tag{22}$$

where the phase differences, θ_k, between the wavenumber components is a uniformly distributed random variable. Fig. 9 shows the waterfall plot of this pressure field. The wavenumber–frequency analysis of this field is shown at Fig. 10. Distinct peaks at the wavenumber $k = \omega/U_c$ are clearly seen, as expected.

A simulated transition region wall pressure field is described by

$$p_{\text{tran}}(x,t) = G(t,x)\sum_k A(k)\, e^{ik(x-U_c t)+\theta_k}. \tag{23}$$

The growth and decay function is composed of a series of exponential functions which are randomly spaced in time to simulate the random creation of the spots. The function $G(t, x)$ indicates the turbidity of the flow with values that range between 0 and 1 (this function is not to be confused with the indicator function of

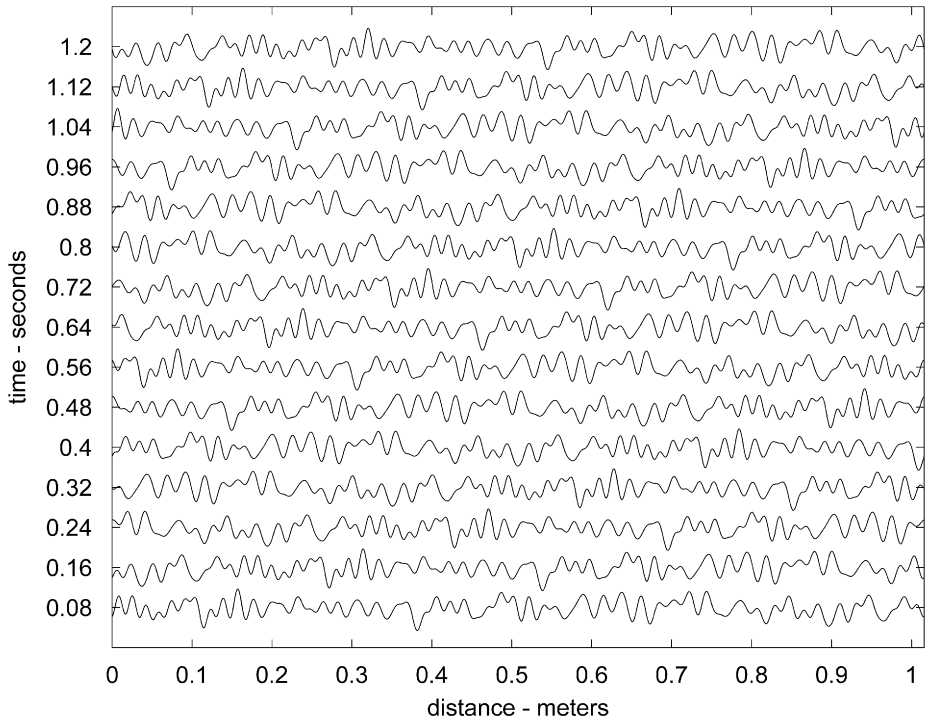

Fig. 9. Waterfall plot of the simulated wall pressure field under a turbulent boundary layer with mean convection velocity U_c.

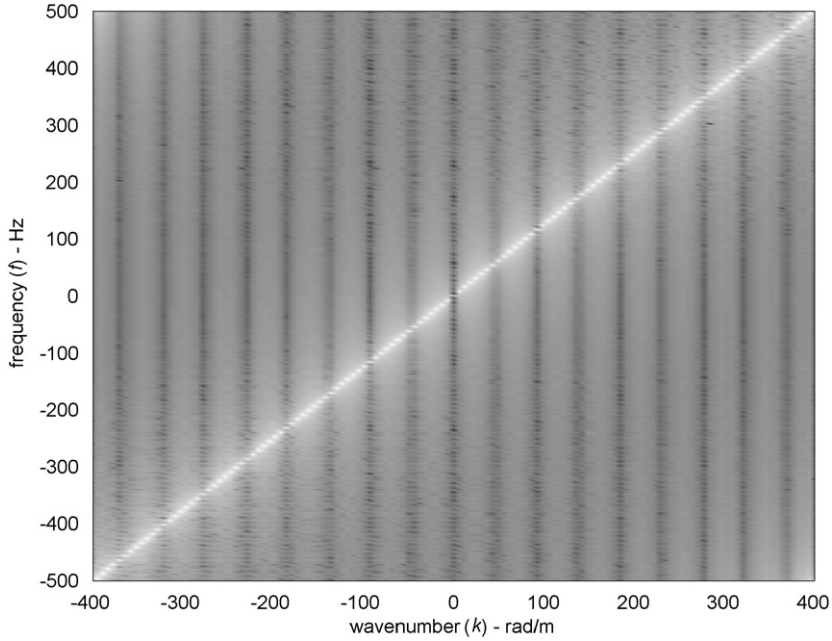

Fig. 10. Wavenumber–frequency spectrum for the simulated wall pressure field under a turbulent boundary layer with mean convection velocity U_c.

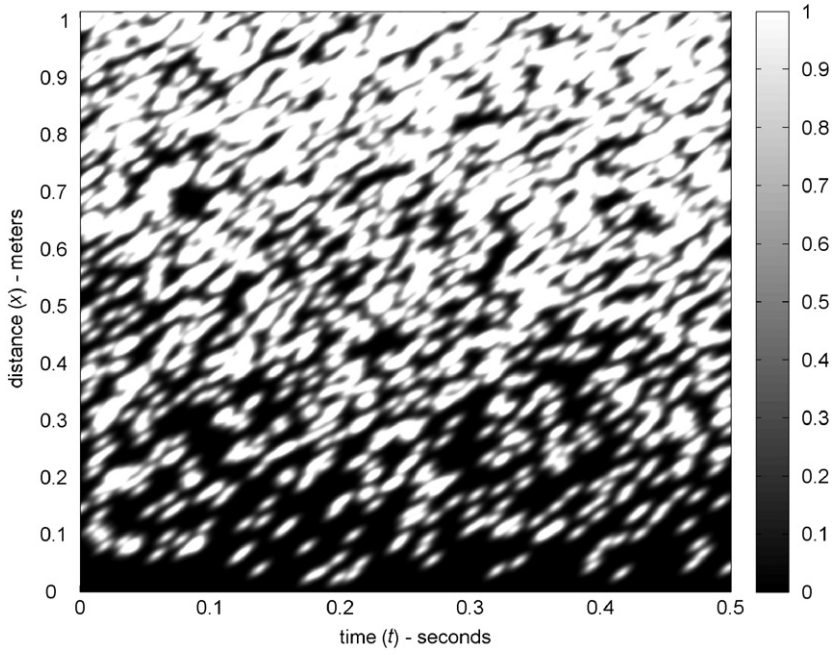

Fig. 11. Growth and decay function $G(t, x)$, where x is streamwise coordinate inside of the transition zone.

Section I, which is a discrete function). It is numerically calculated as follows: at the beginning of the transition zone ($x = x_0$), a turbulent pressure disturbance is created at time t_0. This pressure disturbance is transported downstream while it grows and decays. At some small distance into the transition zone ($x = x_1$), additional pressure disturbances are also created. The rate of pressure disturbances creation increases with x within the

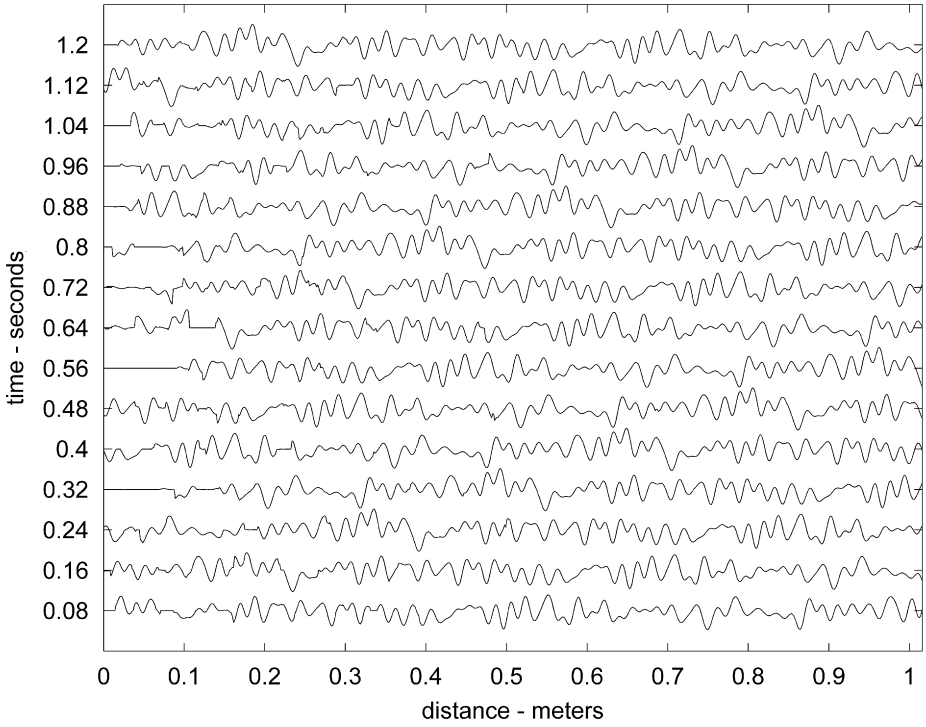

Fig. 12. Waterfall plot of the simulated wall pressure field under a transition zone.

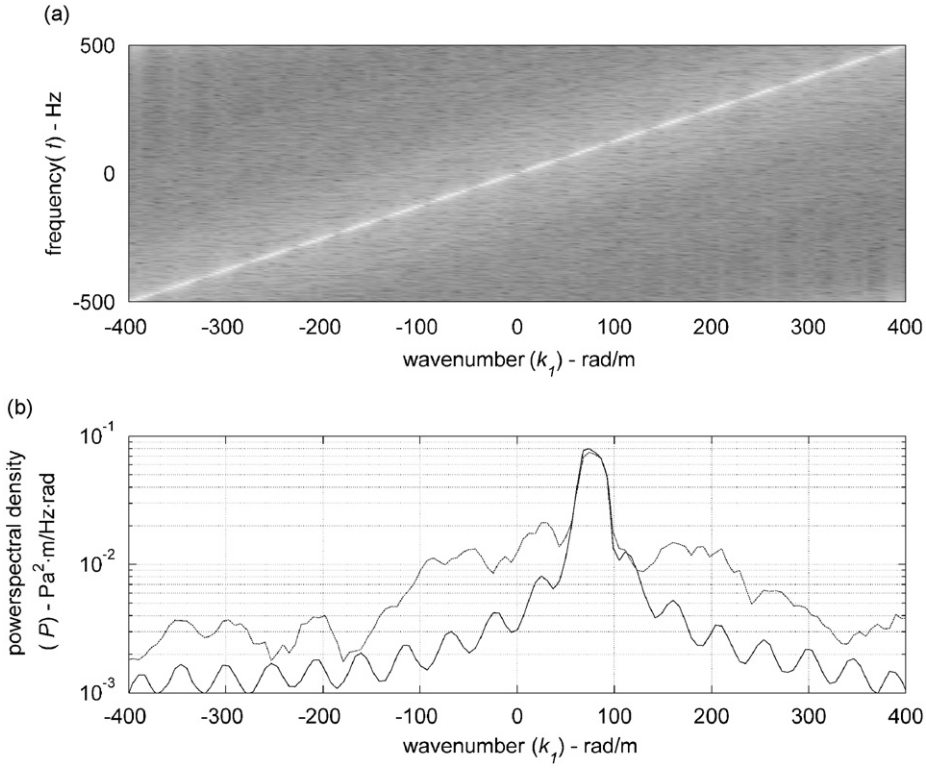

Fig. 13. (a) Wavenumber–frequency spectral analysis for the simulated wall pressure field under a transition zone. (b) Wavenumber spectrum of the transition zone compared to that of the turbulent boundary layer for 100 Hz. (____) Fully turbulent region; (------) transition region.

zone. Three parameters control the function $G(t, x)$: the rate of turbulent pressure disturbance creation, the convection velocity, and the growth/decay function for turbulent pressure disturbances.

The growth function for each individual disturbance follows the form used by Sandham et al. [17]:

$$\ln A = \begin{cases} \dfrac{\sigma_0 \Delta}{2} + \sigma_0 t & \text{for} \quad t < -\Delta \\ -\dfrac{\sigma_0 t^2}{2\Delta} & \text{for} \quad -\Delta < t < \Delta \\ \dfrac{\sigma_0 \Delta}{2} - \sigma_0 t & \text{for} \quad t > \Delta \end{cases}. \tag{24}$$

Fig. 11 shows the simulated growth and decay function $G(t, x)$ in the transition region. This function is applied to the fully turbulent wall pressure field to simulate the wall pressure field in the transition zone. Fig. 12 shows the simulated pressure field in the transition zone. The wavenumber–frequency spectrum is shown in Fig. 13(a). Just as in Fig. 6, the convective wavenumber peaks are spread to the neighboring wavenumbers. Fig. 13(b) shows the wavenumber comparison between the fully turbulent region and transition region at a constant frequency. This comparison is analogous to that of Fig. 7.

6. Conclusions

In this paper we have used experimentally determined space–time correlations for the intermittency function [8] that describe the growth and coalescence of turbulent spots in a naturally occurring subsonic boundary-layer transition zone to model the wavevector–frequency spectrum of the transition zone wall pressure fluctuations. The model assumes that the space–time characteristics of the wall pressure fluctuations within individual spots follow the Corcos [11] model for pressure fluctuations under a fully developed turbulent boundary layer, and that this process is statistically independent of the indicator function process. The wavevector–frequency spectrum of the transition zone wall pressure fluctuations is thus the convolution of the wavevector–frequency spectrum of the intermittency function with that of the turbulent boundary-layer wall pressure fluctuations.

We have also simulated numerically the transition zone wall pressure field using a recently developed model for sound radiation from exponentially growing and decaying subsonic wave fields [17]. It is assumed that the growing and decaying wave fields are wavenumber white. The resulting computations of the wavenumber–frequency spectra agree quite favorably with those of the correlation function model. Furthermore, for a presumed transition zone and fully developed turbulent boundary layer at the same location and Reynolds number, we conclude:

(1) At a fixed frequency, the low-streamwise wavenumber wall pressure components under transition are larger than those under the turbulent boundary layer for transition zone statistical reference locations $\geqslant 0.5\Delta x$, where Δx is the transition length. This may be due to the fact that the spot formation rate (frequency of occurrence) peaks near $0.5\Delta x$.
(2) At the same fixed frequencies, the spanwise wavenumber wall pressure components are less than or equal to those of the turbulent boundary layer, depending on the reference location.
(3) The engineering relevance of these findings is that the wall pressure fluctuations induced by transitional boundary layers may act as efficient forcing functions to real structures that support resonant frequencies and flexural wavenumbers that fall within the low-wavenumber region of the subject calculations. The directly radiated sound from the transition zone may also be greater than that of a turbulent boundary layer of equal area. The fluid–structure coupling and direct radiation from transition could result in increased structural vibration, far-field radiation, and sensor self-noise, for sensors mounted in the structure.

References

[1] M.S. Howe, *Acoustics of Fluid–Structure Interactions*, Cambridge University Press, London, 1998.
[2] W.K. Blake, *Mechanics of Flow-induced Sound and Vibration*, Vols. I and II, Academic Press, Orlando, 1986.

[3] T.M. Farabee, An Experimental Investigation of Wall Pressure Fluctuations Beneath Non-equilibrium Turbulent Boundary Layers, PhD Thesis, Catholic University of America, 1986.
[4] G.C. Lauchle, Hydroacoustics of transitional boundary-layer flow, *Applied Mechanics Review* 44 (1991) 517–531.
[5] G.C. Lauchle, H.L. Petrie, D.R. Stinebring, Laminar flow performance of a heated body in particle-laden water, *Experiments in Fluids* 19 (1995) 305–312.
[6] S. Dhawan, R. Narasimha, Some properties of boundary layer flow during the transition from laminar to turbulent motion, *Journal of Fluid Mechanics* 3 (1958) 418–436.
[7] G.C. Lauchle, G.B. Gurney, Laminar boundary-layer transition on a heated underwater body, *Journal of Fluid Mechanics* 144 (1984) 79–101.
[8] M.A. Josserand, G.C. Lauchle, Modeling the wavevector–frequency spectrum of boundary-layer wall pressure during transition on a flat plate, *Transactions of the American Society of Mechanical Engineering—Journal of Vibration and Acoustics* 112 (1990) 523–534.
[9] T.M. Farabee, M.J. Casarella, F.C. DeMetz, Source distribution of turbulent bursts during natural transition, Report SAD 89E1942, David W. Taylor Naval Ship Research and Development Center, 1974.
[10] C.J. Gedney, P. Leehey, Wall pressure fluctuations during transition on a flat plate, *Transactions of the American Society of Mechanical Engineering—Journal of Vibration and Acoustics* 113 (1991) 255–266.
[11] G.M. Corcos, The structure of the turbulent pressure field in boundary layer flows, *Journal of Fluid Mechanics* 18 (1964) 353–378.
[12] R.I. Ochsenknecht, Estimation of the Wavenumber–Frequency Spectra for the Non-homogeneous Streamwise Transition Flow Pressure Field, Master of Science Thesis, Penn State University, 1996.
[13] W.A. Strawderman, Wavevector–Frequency Spectra with Applications to Acoustics, US Government Printing Office, Washington, DC, undated.
[14] R.L. Streit, A discussion of Taylor weighting for continuous apertures, Technical Memorandum 851004, Naval Underwater Systems Center, New London, CT, 1985.
[15] J. Audet, Ph. Dufourcq, M. Lagier, Fluctuating wall pressures under a boundary layer during the transition to turbulence, *Journal Acoustique* 2 (1989) 369–378 (in French).
[16] Ph. Dufourcq, Influence of Boundary Layer Flow on the Wall Sound Radiation, Doctoral Thesis, Ecole Centrale de Lyon, 1984 (in French).
[17] N.D. Sandham, C.L. Morfey, Z.W. Hu, Sound radiation from exponentially growing and decaying surface waves, *Journal of Sound and Vibration* 294 (2006) 355–361.